Phonon anomalies and elastic constants of cubic NiAl from first principles

Xiangyang Huang, Ivan I. Naumov, and Karin M. Rabe
Department of Physics and Astronomy, Rutgers University, Piscataway, New Jersey 08854-8019, USA
(Received 23 March 2004; published 20 August 2004)

The phonon dispersion relation of NiAl in the cubic *B*2 structure is calculated using first-principles density-functional perturbation theory with pseudopotentials and a plane-wave basis set. Anomalies are present in acoustic branches along three major symmetry directions: Γ-*X*, Γ-*M*, and Γ-*R*, with the positions being in excellent agreement with experiment. Analysis of the Fermi surface and the generalized susceptibility shows that these are Kohn anomalies. Overall, the computed phonon frequencies significantly decrease with increasing lattice parameter. This unusual sensitivity is attributed to a two-dimensional van Hove singularity in the electronic density of states near the Fermi level. The phonon dispersion is compared with that of *B*2 NiTi, and the origin of phonon anomalies in the high-temperature phase is found to be different in the two systems.

DOI: 10.1103/PhysRevB.70.064301 PACS number(s): 63.20.Dj, 71.18.+y, 71.20.Be

I. INTRODUCTION

Active materials, such as piezoelectric oxides and shape-memory alloys, have been the subject of intensive investigation due to their favorable electro- and thermo-mechanical properties. Ni-based shape-memory alloys including NiTi, Ni_xAl_{1-x}, and ferromagnetic Ni_2MnGa have attracted particular attention because they have been shown to be quite useful in the design of mechanical actuator devices.[1] The "active" character of these systems is connected to a reversible martensitic transformation. The phonon dispersion of the high-symmetry high-temperature phase generally exhibits anomalous softening, localized in reciprocal space, in one or more acoustic phonon branches, and particular elastic constants may in addition show strong temperature dependence. As the temperature decreases, these can lead to instability of the high-temperature structure, often observed to be preempted before softening is complete by a first-order transition to the lower symmetry martensite phase.

Two different mechanisms by which phonon anomalies can develop in shape-memory alloys have been proposed. The first is related to the geometry of the Fermi surface, leading to a so-called Kohn anomaly.[2] In this case, the perturbation potential due to atomic displacements at a particular wave vector $\mathbf{q}$ is strongly screened by low-energy electronic transitions from occupied states at $\mathbf{k}$ to unoccupied states at $\mathbf{k}+\mathbf{q}$. The strength of the anomaly depends on the phase space for such transitions, which is large when sheets of the Fermi surface are nested by $\mathbf{q}$. Alternatively, an anomaly may be produced by large values for the relevant electron-phonon matrix elements.[3] Gooding and Krumhansl have argued that the coupling of the anomalous phonon to strain is a key element in describing its relationship to the low temperature phase.[4] Using Laudau theory, they proposed that phase transition can occur via incomplete softening of a phonon branch (nonzero frequency or not even close to zero), strong anharmonic interaction between this phonon and strain can still lead to a first-order phase transition.

The extent to which these mechanisms are relevant can only be determined by a detailed study of the material of interest. Here, we consider stoichiometric NiAl. The β-phase structure of Ni_xAl_{1-x} alloys is well known to exhibit a martensitic transformation for x from 0.60 to 0.65 (Ref. 5). Using inelastic neutron diffraction, the phonon dispersion of alloys with $0.5<x<0.65$ have been studied and an anomaly in the transverse acoustic TA_2 branch along the [110] direction has been observed. Close examination of phonon dispersion of stoichiometric NiAl reveals weaker anomalies also exist in [100] and [111] directions.[6] The position of the anomaly shifts towards Γ as *x* increases in this range. At the same time, the elastic constant c', associated with the long wavelength ($\mathbf{q}\sim 0$) limit of the TA_2 mode, is lowered dramatically.[7–9] In the range of $0.60\leqslant x\leqslant 0.64$, as the temperature decreases the TA_2 mode at $\pi/a(\frac{1}{3},\frac{1}{3},0)$ softens. Subsequently, there is a first-order transition to an intermediate monoclinic 7*R* "sevenfold" premartensitic structure, [10] which at still lower temperature undergoes a further transition to the tetrogonal 3*R* structure. [11]

Eighteen years ago, Shapiro *et al.*[5] proposed that the phonon anomaly in the [110] TA_2 branch is of electronic origin. Subsequently, it was suggested that the key ingredient is the Fermi surface nesting at the wave vector of the anomaly.[6] Theoretical analysis requires relating the elastic constants, the phonon dispersion, the electronic structure, and the strain. The electronic origin of the anomaly in cubic NiAl was supported by the semiempirical analysis of Ref. 13, which used the Varma and Weber[3] approach to decompose the dynamical matrix into short-range and band structure contributions. The latter, fit to first-principles linear combination of atomic orbitals band structure results, were shown to be responsible for the anomaly through nesting of portions of the Fermi surface in the seventh band. This contribution also produced anomalies in acoustic branches along other directions including Γ-*X* and Γ-*R*. Naumov and Velikokhatniy[12] argued that the softening of the elastic constant c' also has an electronic origin related to the presence of a two-dimension van Hove singularity in the electronic density of states below the Fermi level. Using linear muffin-tin orbital (LMTO) calculations of the density of states in *B*2 NiAl, they obtained the electronic contribution to the elastic constant c' and found that as the separation $\eta=\varepsilon_F-\varepsilon_C$ between the Fermi level and the energy of the 2D van Hove singularity decreases, the [110] TA_2 phonon branch undergoes an overall softening.

It is worth noting that another shape-memory alloy, NiTi, has the same $B2$ structure in high temperature and also shows a TA_2 anomaly along [110] direction. The simularity of the TA_2 phonon anomalies in both alloys led many investigators to conjecture that these anomalies have the same origin.[13,14] It is of particular interest to clarify this from a detailed first-principles study. In this paper, we report a fully first-principles investigation, with calculations of the elastic constants, the phonon dispersion, and the electronic structure of $B2$ NiAl, and the coupling to strain. In Sec. II. we specify the technique used in the first-principles calculations. In Sec. III, we present the computed structure, elastic constants, and phonon dispersion of NiAl. The nature of observed anomalies are then investigated by analyzing the Fermi surface and the generalized susceptibility. A comparison of the phonon anomalies in NiAl with those in NiTi is made. A 2D van Hove singularity is identified in the electronic density of states, and this feature is proposed as the main origin of the sensitivity of the computed phonon frequencies to the lattice parameter. We conclude the paper in Sec. IV.

II. COMPUTATIONAL DETAILS

First-principles calculations of the structural energetics of $B2$ NiAl were carried out within density-functional theory with a plane-wave pseudopotential approach. Phonon eigenfrequencies and eigenvectors throughout the Brillouin zone (BZ) were obtained using density-functional perturbation theory.[15] The calculations were performed with the PWSCF and PHONON codes,[16] using the Perdew-Zunger[17] parametrization of the local-density approximation (LDA). Ultrasoft pseudopotentials[18] for Ni and Al were generated according to a modified Rappe-Rabe-Kaxiras-Joannopoulos scheme[19] with three Bessel functions.[20] The electronic wave functions were expanded with a plane-wave basis set with a kinetic energy cutoff of 30 Ry. The augmentation charges were expanded up to 480 Ry. The BZ integrations were carried out by the Hermite-Gaussian smearing technique[21] using a $20\times20\times20$ Monkhorst-Pack (MP) k-point mesh (corresponding to 220 k-points in the irreducible BZ). The value of the smearing parameter was $\sigma=0.01$ Ry. These parameters yield phonon frequencies converged within 1%. The phonon frequencies were calculated along Γ-X, Γ-M, and Γ-R directions for the **q**-points that are commensurate with the **k**-point mesh. This gives 11 points along each direction. A spline fit was used to plot the phonon dispersion curves; the interpolation method based on computation of real-space force constants require a very dense q-mesh for metals with phonon anomalies, which is numerically very expensive and therefore not used in this work.

The generalized susceptibility of noninteracting electrons

$$\chi(\mathbf{q}) = \frac{2\Omega}{(2\pi)^3}\sum_{n,n',\mathbf{k}} f(\varepsilon_{n,\mathbf{k}})\frac{[1-f(\varepsilon_{n',\mathbf{k}+\mathbf{q}})]}{\varepsilon_{n',\mathbf{k}+\mathbf{q}}-\varepsilon_{n,\mathbf{k}}}, \tag{1}$$

was chosen to quantify the nesting features of Fermi surface, where Ω is the volume of the unit cell, $f(\varepsilon)$ is the Fermi-Dirac distribution function and $\varepsilon_{n,\mathbf{k}}$ is the nth band energy at **k**. This function was calculated using the highly precise analytic tetrahedron method,[22] with no artificial broadening technique involved. The whole BZ is divide by $50\times50\times50$ regular mesh along the k_x, k_y, and k_z axes, corresponding to 15 625 tetrahedra in the irreducible BZ.

Two different approaches were used to calculate the elastic constants of NiAl. Elastic constants obtained by calculating the energy change associated with small deformations of the unit cell are refered to as "static" elastic constants. A $20\times20\times20$ Monkhorst-Pack (MP) **k**-point mesh and tetrahedron method were used in the total energy calculations. The following deformation matrices are constructed to evaluate B, c', and c_{44}, respectively,

$$\begin{pmatrix} 1+\epsilon & 0 & 0 \\ 0 & 1+\epsilon & 0 \\ 0 & 0 & 1+\epsilon \end{pmatrix}, \tag{2}$$

$$\begin{pmatrix} (1+\epsilon)^{1/3} & 0 & 0 \\ 0 & (1+\epsilon)^{1/3} & 0 \\ 0 & 0 & (1+\epsilon)^{-2/3} \end{pmatrix}, \tag{3}$$

$$\begin{pmatrix} 1 & \epsilon & \epsilon \\ \epsilon & 1 & \epsilon \\ \epsilon & \epsilon & 1 \end{pmatrix}. \tag{4}$$

Particularly, we have $\delta E=\frac{9}{2}B\epsilon^2$, $\delta E=\frac{2}{3}c'\epsilon^2$ and $\delta E=6c_{44}\epsilon^2$ corresponding to the above three matrices.

Alternatively, elastic constants can be obtained from the slopes of the acoustic phonon branches in the long wavelength limit, refered to as "dynamical elastic constants" in this paper. In the cubic structure, all three elastic constants can be determined from the slopes of the three acoustic branches along Γ-M:[23] $c_{44}=\rho\omega_{T1}^2/k^2$, $c'=\rho\omega_{T2}^2/k^2$, and $c_L=\rho\omega_L^2/k^2$, where $c'=(c_{11}-c_{12})/2$, $c_L=(c_{11}+c_{12}+2c_{44})/2$, and

TABLE I. Lattice parameter (in a.u.) and elastic constants ($\times10^{12}$ dyn/cm^2) of $B2$ NiAl. The computed values are denoted by PW. The PW value of lattice parameter is $a_0=5.328$ a.u., comparing to the experimental value of 5.455 a.u. (Ref. 24); the corresponding elastic constants were computed at both theoretical and experimental lattice constants using Eqs. (2)–(4) or slopes of three acoustic phonon frequencies (in parentheses). The (USPE) values of elastic constants were determined by ultrasonic pulse-echo method at 298 K (Ref. 8) while the (NS) values of elastic constants were determined by the slopes of measured acoustic phonon frequencies from Ref. 6 at 296 K. Only three of the elastic constants are independent.

	PW	PW	USPE	NS
a_0	5.328	5.455		
B	1.87	1.50	1.58	1.451
c_{11}	2.36	1.89	1.99	1.968
c_{12}	1.67	1.31	1.37	1.192
c_{44}	1.40 (1.36)	1.07	1.16	1.1
c_L	3.42 (3.31)	2.94	2.84	2.68
c'	0.35 (0.43)	0.29	0.31	0.388

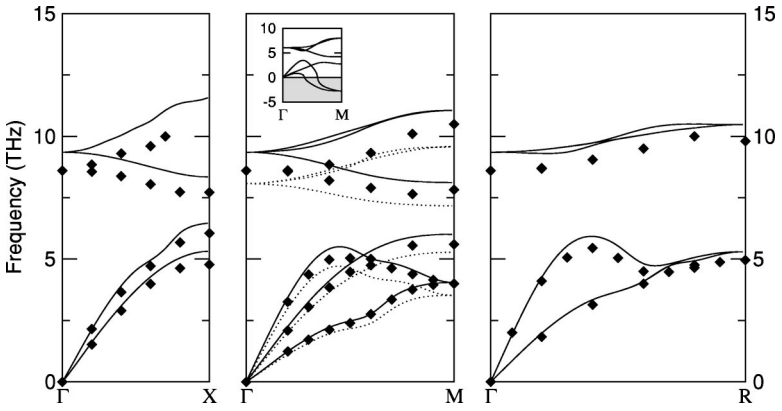

FIG. 1. Phonon dispersion for NiAl in the $B2$ structure with $a_0=5.328$ a.u. (solid lines) and $a_0=5.455$ a.u. (dotted lines) along three high symmetry lines in the simple cubic BZ. Filled diamonds indicate neutron scattering data from Ref. 6. Insetted figure is phonon dispersion for NiTi in the $B2$ structure along [110] direction, which is feathered by a dominant lattice instability at M point.

ρ is the mass density. Under harmonic approximation, the two approaches will give the same elastic constants.

III. RESULTS AND DISCUSSION

The first-principles lattice parameter of $B2$ NiAl is 5.328 a.u., which is 2.4% less than the experimental (at 298 K) value of 5.455 a.u. (Ref. 24) To understand the origin of this rather large discrepancy, we performed full-potential linearized-augmented-plane-wave calculations (FLAPW) with both the LDA and the generalized gradient approximation (GGA).[25] Our LDA pseudopotential result is only slightly smaller than the FLAPW LDA result of 5.359 a.u. The lattice parameter given by FLAPW GGA is 5.476 a.u., which is larger than the experimental value by about 0.4%. The underestimation of the equilibrium lattice parameter is therefore mainly attributable to the local-density approximation.[26] Unless otherwise mentioned, the first-principles lattice parameter is used throughout this paper.

In Table I, we present the structure and elastic constants of $B2$ NiAl as computed from first principles, with corresponding experimental values. The calculated values are generally in good agreement with experiment. Systematic overestimation of elastic constants is expected from the use of the theoretical lattice parameter, so that the near exact agreement of c' should be considered fortuitous. A better agreement of elastic constants is obtained when experimental lattice constant is used. It should be noted that c' is much less than c_{44}, which lowers the accuracy to which it can be determined, and reflects the large elastic anisotropy of this system. Both calculated and experimental results show that the elastic constants computed with the two approaches are reasonably consistent.

The full phonon dispersion of $B2$ NiAl has six branches: three acoustic and three optic. The calculated phonon dispersion curves of NiAl along three high-symmetry lines of the simple cubic BZ, Γ-X, Γ-M, and Γ-R, are shown in Fig. 1 along with that experimentally measured by neutron scattering. The calculated result is in excellent agreement with the experiment for the acoustic branches, while the optic branches appear to be uniformly slightly shifted in frequency. All phonons have $\omega^2 \geq 0$ which is consistent with the fact that NiAl in the $B2$ structure is experimentally observed to be stable down to low temperature.

Close examination of Fig. 1 shows the presence of anomalous dips in the transverse acoustic (TA) branch along Γ-M and Γ-R directions and in the longitudinal acoustic (LA) branch along the Γ-X direction. The positions are consistent with the anomalously low values for experimental phonon frequencies in those branches. To find out whether the anomalies have an electronic origin, we need to know the electronic band structure of NiAl. The band structure of cubic NiAl along high symmetry lines in the simple cubic BZ is shown in Fig. 2. NiAl contains 13 valence electrons per unit cell with only the sixth and seventh bands being partially occupied. The band structure is characterized by a wide Al $s-p$ band, intersected by narrow d bands associated with Ni and located about 2 eV below the Fermi level. This result is very similar to that of the full-potential LMTO result in Ref. 12.

The calculated generalized susceptibility [Eq. (1)] along Γ-X, Γ-M, and Γ-R is shown in Fig. 3. A peak is observed in each of the three directions. Detailed analysis of the partial contributions indicates that the peaks are due to seventh to seventh electron transitions (intraband transitions), shown as dotted lines in Fig. 3; the remaining contribution to the susceptibility, shown as dashed lines is fairly wave vector independent. The nesting vectors are determined to be $\pi/a(0.3,0,0)$, $\pi/a(0.27,0.27,0)$, and $\pi/a(0.25,0.25,0.25)$, which correspond well to the positions of the anomalies. The portions of the calculated Fermi surface due to the seventh band in the planes parallel to ΓXM with $0.1(2\pi/a)$,

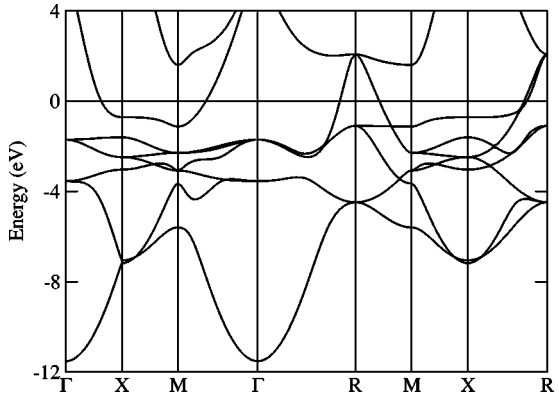

FIG. 2. Calculated band structure for NiAl in the simple cubic BZ, with $a_0=5.328$ a.u.

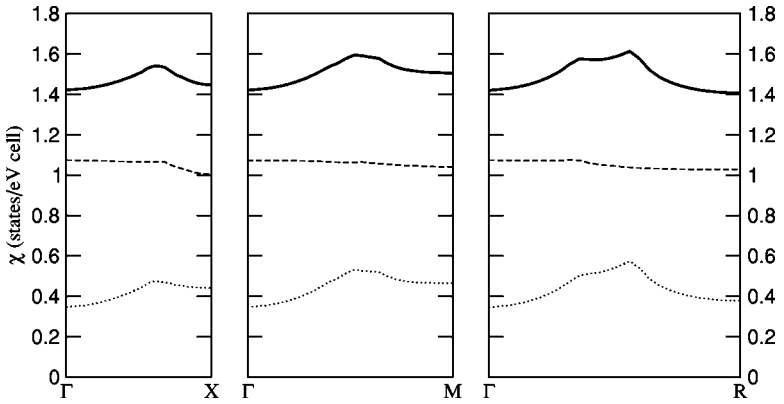

FIG. 3. Calculated generalized susceptibility of *B*2 NiAl along Γ-*X*, Γ-*M*, and Γ-R directions. Solid lines, dotted lines, and dashed lines represent total, the contribution from intraband (Seventh to seventh) electron transition, and remaining contribution, respectively.

$0.3(2\pi/a)$, and $0.5(2\pi/a)$, are shown in Fig. 4. The nesting feature can be clearly seen in the Fermi surface with $k_z = 0.3(2\pi/a)$. The phonon anomalies under discussion are therefore identified to be of the Kohn type. Our results confirmed the validity of the previous semiempirical analysis of the dynamical matrix by Zhao and Harmon.[13] The positions of the anomalies are in good agreement with their results.

It can be seen that the calculated phonon frequencies in Fig. 1 are systematically larger than experiment, the effect being especially pronounced for the optic branches. As for the elastic constants, at least part of this difference might be attributed to the underestimated theoretical lattice constant. We recomputed the phonon dispersion using the experimental lattice parameter of 5.455 a.u. (shown as dotted lines in Fig. 1). This change in the lattice parameter of 2.4% results in reduction of about 15% in the phonon frequencies (see Table II). In fact, the effect is so large as to result in an underestimate of the phonon frequencies. Since the elastic constants, c_{44}, c', and c_L, are proportional to squares of the slopes of acoustic phonons along Γ-*M* in the long wavelength limit, it is clear that the elastic constants are sensitive to the lattice parameter in this alloy.

The anomalies present at the theoretical lattice parameter are essentially unchanged in wave vector and strength by the expansion. This is consistent with a Kohn character of the anomaly, as the Fermi surface is not expected to change significantly. The overall phonon softening can be shown to have an electronic origin associated with features in the occupied electronic density of states (DOS). In Fig. 5, we show the total electronic DOS in the vicinity of the Fermi level for the two different lattice parameters. The DOS is characterized by a peak below the Fermi level, which can be identified as a 2D van Hove singularity, as explain below. Since the *XM* line is the intersection of two symmetry planes, i.e., *XMRM* and *XMX*Γ, transverse (perpendicular to *XM*) electron velocities are zero. The fact also holds for the *XR* line, which is the intersection of another two symmetry planes, i.e., *XRM*Γ and *XMRM*. Due to the hybridization of Al $s-p$ and Ni *d* electrons, the bands along, the *XM* and *XR* lines are rather flat below the Fermi level, therefore, the corresponding van Hove singularity gains 2D character (for more details see Ref. 12).

It is well known that usual 3D van Hove singularity in DOS effects the phonon frequencies for long wavelength limit. It was shown in many works[27] that as the Fermi level approaches the 3D van Hove singularity the phonon frequency squared gains the nonanalytical part $\delta\omega^2(\mathbf{q})$, which exists at one side of the Fermi surface topology changes. From a physical point of view, it is clear that 2D singularity effects in $\omega^2(\mathbf{q})$ are much stronger than the 3D one. As was shown by Vaks and Trefilov,[28] in the case of 2D singularity the long wavelength behavior of the singular part becomes $\delta\omega^2(\mathbf{q}) \sim \ln|\eta|$, where η is the separation between the Fermi level and the energy of the 2D van Hove singularity. Moreover, the entire phonon dispersion curves gain the critical contribution $\delta\omega^2(\mathbf{q}) \sim \delta n(\epsilon_F)$ along the q-lines parallel to those along which electron bands have no dispersion. In the NiAl alloy there are two lines of this kind: [100] and [110]. One may expect especial softening of $\omega^2(\mathbf{q})$ along these lines as the parameter $|\eta|$ approaches to zero. It is easily seen from Fig. 5 that as the lattice parameter increases the Fermi level approaches the peak in the DOS. However, this effect is rather weak in Ni_xAl_{1-x} with different Ni concentration since the change of lattice constants is less than 1% as *x* increases from 0.5 to 0.625. What happens in reality is that the substitution of the Ni for Al leads to a change in the number of conduction electrons and therefore the Fermi level (for more details see Ref. 12). As *x* increases, the Fermi level approaches the van Hove peak and all elastic constants soften. But among the others the constant $c'(x)$ softens dramatically—by a factor of 2.2, 10, and 14 from different authors.[7–9] This is due to the fact that the elastic constant c' is directly related with the transverse acoustic mode TA_2 along [110] direction.

When uniaxial-stress is applied to NiAl along the [001] direction, the initial van Hove peak in DOS splits into two peaks,[12] one of which moves away from the Fermi level while the other approaches it. Analysis shows that this will lead to overall softening in the TA_2 along [110] but not along [011]. Therefore, one may expect significant softening in elastic constant $c'_\perp$ associated with the TA_2 [110], but not with $c'_\parallel$ associated with the TA_2 [101] (or [011]). To check the validity of this analysis, we performed the calculations on tetragonal-distorted structure with volume being constrained to the cubic one. Our results show that when c/a is changed to 0.98, the "dynamic" elastic constant $c'_\perp$ decreases 20% (!) while $c'_\parallel$ has almost no change, which is in agreement with the experiment.[29]

Figure 6 shows TA_2 phonon branch is dramatically affected by tetragonal distortion while the position of anomaly

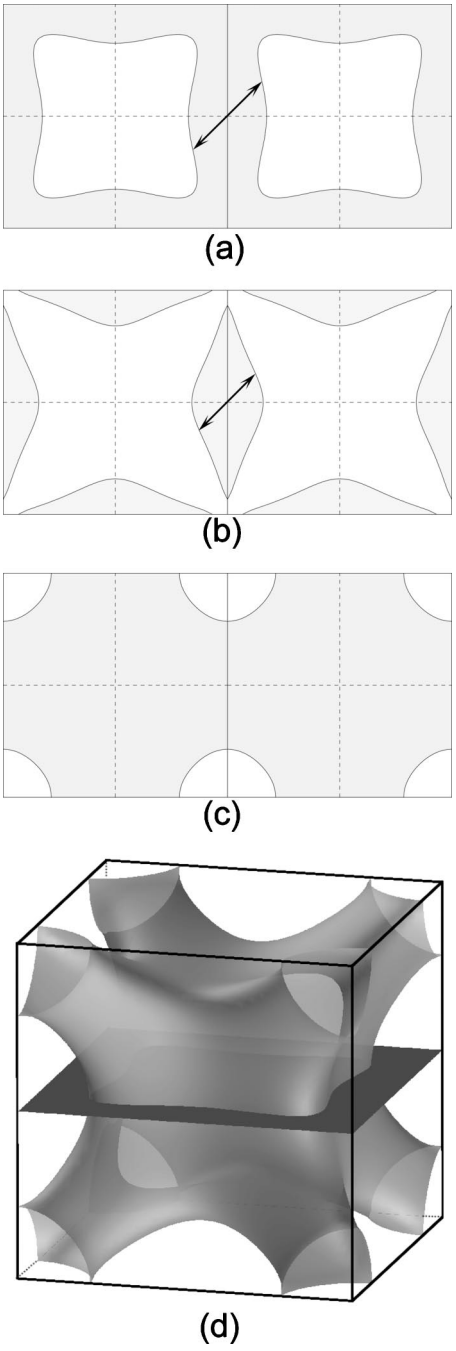

FIG. 4. Portions of the Fermi surface of the seventh band for $B2$ NiAl: (a)–(c) in the planes parallel to ΓXM with $0.1(2\pi/a)$, $0.3(2\pi/a)$, and $0.5(2\pi/a)$ in the extended BZ, respectively, and (d) 3D BZ with a cutting plane. The shaded regions correspond to occupied states and the arrow lines denote nesting vectors.

is almost unchanged. This suggests the interaction between the c' (uniaxial strain) and TA_2 phonon is large in this system.

It is of particular interest to compare phonon dispersion of NiAl with that of NiTi, which likewise has a $B2$ structure in high temperature and also shows a TA_2 anomaly along [110]. Moreover, under cooling the TA_2 phonon condenses at $\pi/3a$ [110] bringing into existence the so-called R-phase, which is

TABLE II. Computed phonon frequencies (in THz) of $B2$ NiAl with $a_0=5.328$ a.u. and $a_0^1=5.455$ a.u. at the high symmetry points, comparing with the experimental results from Ref. 6.

Label	a_0	a_0^1	exp.
Γ_{15}	0	0	0
Γ_{15}	9.353	8.074	8.60
$X_{5'}$	5.317	4.699	4.78
$X_{1'}$	6.472	5.648	6.05
X_5	8.345	7.354	7.72
X_1	11.599	10.181	-
$M_{5'}$	4.052	3.554	4.00
$M_{1'}$	6.014	5.270	5.60
$M_{4'}$	8.118	7.173	7.82
$M_{5'}$	11.059	9.566	10.50
R_{15}	5.290	4.439	4.96
R_{25}	10.479	9.239	9.80

analogous to the $7R$-phase in the Ni_xAl_{1-x} system. This similar behavior of the TA_2 phonon modes in these two alloys led many investigators to think that their experimentally observed anomalies are of the same nature, i.e., the Kohn type. Our calculations suggest, however, the phonon anomaly in the NiAl system is related to the local geometry of the Fermi surface and the strong interaction between strain (c') and TA_2 phonon will not change the position of anomalies. But it is not necessarily to be true in the NiTi system. Indeed, our previous investigation on NiTi shows phonon dispersion is feathered by a dominant lattice instability at the M point,[30] shown as the inset in Fig. 1. The distorted structure produced by freezing a particular choice of the unstable $M_{5'}$ eigenvector into the reference cubic structure yields an excellent approximation to the observed ground-state $B19'$ structure. The stability of high-temperature $B2$ structure is due to anharmonic phonon-phonon interactions and the phonons in the

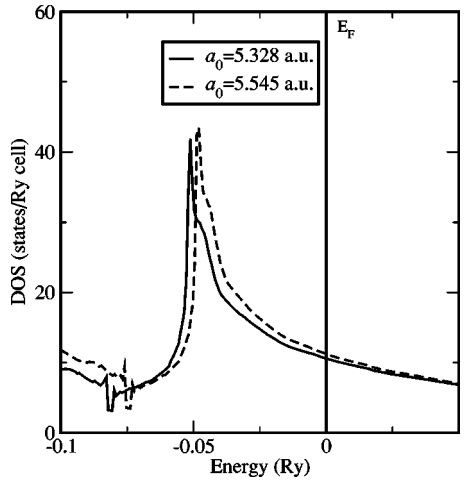

FIG. 5. Total DOS of $B2$ NiAl in the vicinity of the Fermi level with lattice parameters 5.328 a.u. (solid line) and 5.455 a.u. (dotted line). The Fermi level E_F is taken as the zero of energy in each case.

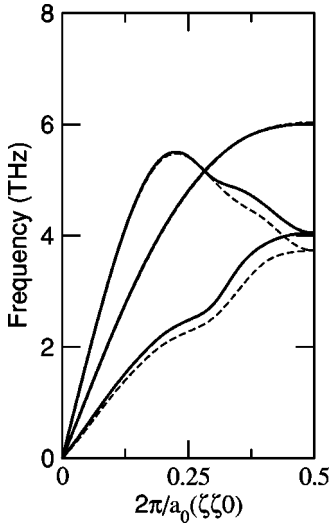

FIG. 6. Calculated acoustic phonon frequencies of NiAl along [110] direction. Solid lines and dashed lines represent undistorted and volume-conserving tetragonal-distorted structure ($c/a=0.98$), respectively.

*B*2 phase are strongly renormalized by these interactions. Zhao and Harmon[31] showed that the Fermi surface nesting effect also contributes the anomalies in NiTi. This makes identification of the origin of the dip in the TA_2 phonon branch in NiTi a bit different than that in NiAl. However, our work suggests that this effect is rather weak in NiTi. The dip in the TA_2 phonon modes forms at $\pi/3a$ [110], which is the case proposed by Gooding and Krumhansl.[32]

IV. CONCLUSIONS

In conclusion, we performed first-principles calculations of the structure, elastic constants, and phonon dispersion of NiAl in the cubic *B*2 structure. Anomalies observed in one of the acoustic branches along three major symmetry directions are found to be due to Fermi surface nesting, and thus can be classified as Kohn anomalies. The high sensitivity of the phonon dispersion to the Ni concentrations (due to number of conduction electrons) can been explained by a corresponding sensitivity of the electronic density of states due to a 2D van Hove singularity near the Fermi level. The phonon dispersion of NiAl is further compared with that of *B*2 NiTi, and the different origin of phonon anomalies in two systems is revealed.

ACKNOWLEDGMENTS

The authors thank R. D. James and K. Bhattacharya for valuable discussions. This work was supported by AFOSR/MURI F49620-98-1-0433. The calculations were performed on the SGI Origin 2000 and IBM SP3 at ARL MSRC.

[1] R. D. James and K. F. Hane, Acta Mater. **48**, 197 (2000).
[2] W. Kohn, Phys. Rev. Lett. **2**, 393 (1959).
[3] C. M. Varma and W. Weber, Phys. Rev. Lett. **39**, 1094 (1977); Phys. Rev. B **19**, 6142 (1979).
[4] R. J. Gooding and J. A. Krumhansl, Phys. Rev. B **38**, 1695 (1988).
[5] S. M. Shapiro, J. Z. Larese, Y. Noda, S. C. Moss, and L. E. Tanner, Phys. Rev. Lett. **57**, 3199 (1986).
[6] M. Mostoller, R. M. Nicklow, D. M. Zehner, S.-C. Lui, J. M. Mundenar, and E. W. Plummer, Phys. Rev. B **40**, 2856 (1989).
[7] K. Enami, J. Hasunuma, A. Nagasawa, and S. Nenno, Scr. Metall. **10**, 879 (1976).
[8] N. Rusovic and H. Warlimont, Phys. Status Solidi A **44**, 609 (1977).
[9] L. Zhou, P. Cornely, J. Trivisonno, D. Lahrman, *IEEE 1990 Ultrasonics Symposium Proceedings* (IEEE, New York, 1990), Vol. 3, p. 1309.
[10] S. M. Shapiro, B. X. Yang, G. Shirane, Y. Noda, and L. E. Tanner, Phys. Rev. Lett. **62**, 1298 (1989).
[11] V. G. Pushin, S. P. Pavlova, and L. I. Yurchenko, Fiz. Met. Metalloved. **67**, 164 (1989).
[12] I. I. Naumov and O. I. Velikokhatniy, J. Phys.: Condens. Matter **9**, 10339 (1997).
[13] G. L. Zhao and B. N. Harmon, Phys. Rev. B **45**, 2818 (1992).
[14] A. Zheludev, S. M. Shapiro, P. Wochner, A. Schwartz, M. Wall, and L. E. Tanner, Phys. Rev. B **51**, 11 310 (1995).
[15] S. Baroni, P. Giannozzi, and A. Testa, Phys. Rev. Lett. **58**, 1861 (1987).
[16] S. Baroni, S. de Gironcoli, A. Dal Corso, and P. Giannozzi, http://www.sissa.it/cm/PWcodes
[17] J. P. Perdew and A. Zunger, Phys. Rev. B **23**, 5048 (1981).
[18] D. Vanderbilt, Phys. Rev. B **41**, 7892 (1990).
[19] A. M. Rappe, K. M. Rabe, E. Kaxiras, and J. D. Joannopoulos, Phys. Rev. B **41**, 1227 (1990).
[20] A. DalCorso, A. Pasquarello, and A. Baldereschi, Phys. Rev. B **56**, R11 369 (1997).
[21] M. Methfessel and A. T. Paxton, Phys. Rev. B **40**, 3616 (1989).
[22] J. Rath and A. J. Freeman, Phys. Rev. B **11**, 2109 (1975).
[23] *Phonons in Perfect Lattices and in Lattices with Point Imperfections*, edited by R. W. H. Stevenson (Plenum Press, New York, 1966), pp. 9–12.
[24] R. J. Wasilewski, Acta Metall. **15**(11), 1757 (1967).
[25] P. Blaha, K. Schwarz, and J. Luitz, WIEN97, Vienna University of Technology, Vienna 1997. (Improved and updated Unix version of the original copyrighted WIEN-code, published by P. Blaha, K. Schwarz, P. Sorantin, and S. B. Trickey, in Comput. Phys. Commun. **59**, 399 1990). Our FLAPW calculations were performed using a 120 *k*-point mesh in the $\frac{1}{48}$ irreducible wedge. No shape approximations were made to the density or potential. A $R_{MT}K_{MAX}$ of 10 were used. The tetrahedron method was used in the BZ integrations.
[26] G. J. Ackland, X. Y. Huang, and K. M. Rabe, Phys. Rev. B **68**, 214104 (2003). According to our first-principles calculations using quasiharmonic approximation, the linear thermal expansion is about 0.32% at 298 K, corresponding to a lattice parameter of 5.345 a.u. at this temperature.

[27] See, for example, L. Dagens, J. Phys. F: Met. Phys. **8**, 2093 (1978).
[28] V. G. Vaks and A. V. Trefilov, J. Phys.: Condens. Matter **3**, 1389 (1991).
[29] S. M. Shapiro, E. C. Svensson, C. Vettier, and B. Hennion, Phys. Rev. B **48**, 13 223 (1993).
[30] X. Y. Huang, C. Bungaro, V. Godlevsky, and K. M. Rabe, Phys. Rev. B **65**, 014108 (2002).
[31] G. L. Zhao and B. N. Harmon, Phys. Rev. B **48**, 2031 (1993).
[32] R. J. Gooding and J. A. Krumhansl, Phys. Rev. B **39**, 1535 (1989).